PAPER

Abundant optical soliton solutions for the stochastic fractional fokas system using bifurcation analysis

To cite this article: Wael W Mohammed *et al* 2024 *Phys. Scr.* **99** 045233

View the article online for updates and enhancements.

IOP Publishing Phys. Scr. 99 (2024) 045233 https://doi.org/10.1088/1402-4896/ad30fd

Physica Scripta

CrossMark

RECEIVED
13 October 2023

REVISED
20 February 2024

ACCEPTED FOR PUBLICATION
6 March 2024

PUBLISHED
18 March 2024

PAPER

Abundant optical soliton solutions for the stochastic fractional fokas system using bifurcation analysis

Wael W Mohammed[1,2,*], **Clemente Cesarano**[3], **Adel A Elmandouh**[2,4], **Ikbal Alqsair**[5], **Rabeb Sidaoui**[1] and **Hessa W Alshammari**[1]

[1] Department of Mathematics, College of Science, University of Ha'il, Ha'il 2440, Saudi Arabia
[2] Department of Mathematics, Faculty of Science, Mansoura University, Mansoura, Egypt
[3] Section of Mathematics, International Telematic University Uninettuno, Corso Vittorio Emanuele II, 39, 00186 Roma, Italy
[4] Department of Mathematics and Statistics, College of Science, King Faisal University, P. O. Box 400, Al-Ahsa 31982, Saudi Arabia
[5] Department of Mathematics, College of Science, Qassim University, Buraydah 51482, Saudi Arabia
[*] Author to whom any correspondence should be addressed.

E-mail: wael.mohammed@mans.edu.eg and c.cesarano@uninettunouniversity.net

Keywords: fractional derivatives, nonlinear system, Wiener process, optical solitons, multiplicative noise

Abstract

In this study, the stochastic fractional Fokas system (SFFS) with M-truncated derivatives is considered. A certain wave transformation is applied to convert this system to a one-dimensional conservative Hamiltonian system. Based on the qualitative theory of dynamical systems, the bifurcation and phase portrait are examined. Utilizing the conserved quantity, we construct some new traveling wave solutions for the SFFS. Due to the fact that the Fokas system is used to explain nonlinear pulse transmission in mono-mode optical fibers, the given solutions may be applied to analyze an extensive variety of crucial physical phenomena. To clarify the effects of the M-truncated derivative and Wiener process, the dynamic behaviors of the various obtained solutions are depicted with 3-D and 2-D curves.

1. Introduction

Stochastic partial differential equations (SPDEs) are mathematical models that explain the behavior of random processes in space and time. They are an extension of ordinary differential equations and partial differential equations, which involve deterministic functions, to include random or stochastic terms SPDEs play a crucial role in many scientific fields, including physics, biology, finance, and engineering, as they provide a powerful tool for understanding complex systems that exhibit randomness [1, 2].

The applications of SPDEs are diverse and far-reaching. In physics, they are used to model the behavior of complex fluids, such as turbulent flows, which exhibit random fluctuations at small scales. In finance, SPDEs are employed to model the dynamics of stock prices, interest rates, and other financial instruments, taking into account the uncertainty and randomness in the market. In biology, SPDEs are used to describe the growth and interaction of populations, where environmental factors and genetic variations introduce stochastic effects.

Solving SPDEs is a challenging task due to the interplay between randomness and spatial-temporal dynamics. In recent years, the exact solutions for some SPDEs, for example coupled Korteweg–De Vries [3], mKdV equation [4], Davey–Stewartson equation [5], $(4+1)$-dimensional Fokas equation [6] and etc, have been acquired.

On the other hand, fractional partial differential equations offer a powerful mathematical framework for modeling complex phenomena that cannot be accurately described by traditional PDEs. By introducing fractional derivatives, FPDEs capture non-local and memory-like effects, enabling them to accurately represent a wide range of scientific phenomena. With implementations in physics, finance, and biomedical engineering [7–11], FPDEs have proven to be a valuable tool for understanding and analyzing complex systems. As a result, multiple mathematicians proposed several fractional derivatives. The most well-known include those suggested by Riemann-Liouville, Riesz, Caputo, Hadamard, two-scale fractal derivative, He's fractional derivative, Grunwald-Letnikov, Atangana-Baleanu's derivative and M-truncated derivative [12–18].

Moreover, solving FPDEs remains a challenging task, requiring the development of specialized analytical methods. In recent years, there are some effective and helpful methods, including modified simple equation method [19], first integral method [20], (G/G') -expansion method [21], extended Jacobi elliptic function expansion method [22], generalizing Riccati equation mapping method [23] , first integral method [24, 25], sine–cosine function method [26], Kudryashov's method [27], and multivariate bilinear neural network method [28], have been developed to solve FPDEs.

In this study, we look at the stochastic fractional Fokas system (SFFS) with M-truncated derivatives:

$$i\mathcal{Y}_t + \gamma_1 \mathbb{D}^{\alpha,\beta}_{k,xx}\mathcal{Y} + \gamma_2 \mathcal{X}\mathcal{Y} = i\sigma\mathcal{Y}\mathcal{W}_t,\ \gamma_3 \mathbb{D}^{\alpha,\beta}_{k,y}\mathcal{X}_y = \gamma_4 \mathbb{D}^{\alpha,\beta}_{k,x}(|\mathcal{Y}|^2), \tag{1}$$

where $\mathbb{D}^{\alpha,\beta}_{k,x}$ is the M-truncated derivative (MTD) operator, $i = \sqrt{-1}$, $\gamma_1, \gamma_2, \gamma_3$ and γ_4 are arbitrary constants. $\mathcal{W} = \mathcal{W}(t)$ is the standard Wiener process, $\mathcal{W}_t = \frac{\partial \mathcal{W}}{\partial t}$ and σ is the amplitude of the noise. When $\alpha = 1$ and $\beta = \sigma = 0$, we get the Fokas system (FS) [29, 30]:

$$i\mathcal{Y}_t + \gamma_1 \mathcal{Y}_{xx} + \gamma_2 \mathcal{X}\mathcal{Y} = 0,\ \gamma_3 \mathcal{X}_y = \gamma_4 (|\mathcal{Y}|^2)_x. \tag{2}$$

Due to the significance of FS (1), many researchers have obtained exact solutions for this equation by using various methods, including generalized Kudryashov method [31], simplified extended tanh-function [32], exp-function method [33], Jacobi elliptic function expansion [34, 35], sine-cosine and extended rational sinh-cosh methods [36], modified mapping method [37], Hirota's bilinear method [38], $\exp(-\psi(k))$ -expansion method [39], Painlevé analysis method [40] and new Kudryashov approach [41].

The goal of this research is to get the exact fractional stochastic solutions of the SFFS (1). Based on the qualitative theory of dynamical systems, the bifurcation and phase portrait are examined. Utilizing the conserved quantity, we construct some new traveling wave solutions for the SFFS. Because the Fokas system is implemented to clarify nonlinear pulse propagation in mono-mode optical fibers, the solutions provided may be utilized to analyze a broad range of critical physical processes. Also, to explain the impacts of the M-truncated derivatives and multiplicative noise, the dynamic behaviors of the different found solutions are illustrated using 3-D and 2-D curves.

The following is how the paper is structured: In the next section, we state the definition of the Wiener process and MTD, while in section 3 we derive the wave equation for the SFFS (1). In section 4, we get the one-dimension conservative Hamiltonian system and its equilibrium points. In section 5, we construct some new traveling wave solutions for the SFFS (1). In section 6, we investigate the effect of the Wiener process on the solutions of SFFS (1). Finally, the conclusion of the article is introduced.

2. Wiener process and MTD

Let us begin by defining the standard Wiener process (SWP) [42]:

Definition 1. The stochastic process $\{\mathcal{W}(s)\}_{s \geqslant 0}$ is known as the SWP if it fulfills:

1. $\mathcal{W}(0) = 0$.
2. $\mathcal{W}(s)$ is continuous for $s \geqslant 0$,
3. $\mathcal{W}(s_2) - \mathcal{W}(s_1)$ is independent for $s_1 < s_2$,
4. $\mathcal{W}(s_2) - \mathcal{W}(s_1)$ has a Normal process,

We need the next lemma for our results:

Lemma 2. *([42])* $\mathbb{E}(e^{\sigma\mathcal{W}(\tau)}) = e^{\frac{1}{2}\sigma^2\tau}$ *for* $\sigma \geqslant 0$.

Recently, Sousa *et al* [18] introduced the M-truncated derivative (MTD), which is a standard generalization of the classical derivatives. They defined the MTD of order $\alpha \in (0, 1]$ for $\mathcal{U}$: $[0, \infty) \to \mathbb{R}$ as follows:

$$\mathbb{D}^{\alpha,\beta}_{k,z}\mathcal{U}(z) = \lim_{h\to 0}\frac{\mathcal{U}(z\mathcal{E}_{k,\beta}(hz^{-\alpha})) - \mathcal{U}(z)}{h},$$

where

$$\mathcal{E}_{k,\beta}(x) = \sum_{p=0}^{k} \frac{x^p}{\Gamma(p\beta + 1)},$$

for $x \in C$ and $\beta > 0$. MTD possesses the following features:

$$(1)\ \mathbb{D}_{k,z}^{\alpha,\beta}(au + bv) = a\mathbb{D}_{k,z}^{\alpha,\beta}(u) + b\mathbb{D}_{k,z}^{\alpha,\beta}(v),$$
$$(2)\ \mathbb{D}_{k,z}^{\alpha,\beta}(u \circ v)(z) = u'(v(z))\,\mathbb{D}_{k,z}^{\alpha,\beta} v(z),$$
$$(3)\ \mathbb{D}_{k,z}^{\alpha,\beta}(uv) = u\mathbb{D}_{k,z}^{\alpha,\beta} v + v\mathbb{D}_{k,z}^{\alpha,\beta} u,$$
$$(4)\ \mathbb{D}_{k,z}^{\alpha,\beta}(u)(z) = \frac{z^{1-\alpha}}{\Gamma(\beta + 1)} \frac{du}{dz},$$
$$(5)\ \mathbb{D}_{k,z}^{\alpha,\beta}(z^\nu) = \frac{\nu}{\Gamma(\beta + 1)} z^{\nu-\alpha},$$

where a and b are any constants.

3. Traveling Wave equation for SFFS

To attain the wave equation for the SFFS (1), we use

$$\mathcal{Y}(x, y, t) = \mathcal{U}(\xi) e^{i\phi + \sigma\mathcal{W}(t) - \frac{1}{2}\sigma^2 t},\ \mathcal{X}(x, y, t) = \mathcal{V}(\xi) e^{\sigma\mathcal{W}(t) - \frac{1}{2}\sigma^2 t},$$

with

$$\phi = \frac{\Gamma(\beta+1)}{\alpha}[\phi_1 x^\alpha + \phi_2 y^\alpha] + \phi_3 t \text{ and } \xi = \frac{\Gamma(\beta+1)}{\alpha}[\xi_1 x^\alpha + \xi_2 y^\alpha] + \xi_3 t, \tag{3}$$

where $\mathcal{U}$ and $\mathcal{V}$ are real and deterministic functions, ϕ_k and ξ_k are unknown constants for $k = 1, 2, 3$. We notice that

$$\begin{aligned}\mathcal{Y}_t &= [\xi_3 \mathcal{U}' + i\phi_3 \mathcal{U} + \sigma\mathcal{U}\mathcal{W}_t + \frac{1}{2}\sigma^2\mathcal{U} - \frac{1}{2}\sigma^2\mathcal{U}] e^{i\phi + \sigma\mathcal{W}(t) - \frac{1}{2}\sigma^2 t}\\ &= [\xi_3 \mathcal{U}' + i\phi_3 \mathcal{U} + \sigma\mathcal{U}\mathcal{W}_t] e^{i\phi + \sigma\mathcal{W}(t) - \frac{1}{2}\sigma^2 t},\end{aligned} \tag{4}$$

where $+\frac{1}{2}\sigma^2\mathcal{U}$ is the Itô correction term, and

$$\begin{aligned}&\mathbb{D}_{k,y}^{\alpha,\beta}\mathcal{Y} = (\xi_1 \mathcal{U}' + i\phi_1 \mathcal{U}) e^{i\phi + \sigma\mathcal{W}(t) - \frac{1}{2}\sigma^2 t},\\ &\mathbb{D}_{k,x}^{\alpha,\beta}(|\mathcal{Y}|^2) = \xi_1 (\mathcal{U}^2)' e^{2\sigma\mathcal{W}(t) - \sigma^2 t},\ \mathbb{D}_{k,y}^{\alpha,\beta}\mathcal{X} = \xi_2 \mathcal{V}' e^{\sigma\mathcal{W}(t) - \frac{1}{2}\sigma^2 t},\\ &\mathbb{D}_{k,xx}^{\alpha,\beta}\mathcal{Y} = (\xi_1^2 \mathcal{U}'' + 2i\phi_1\xi_1 \mathcal{U}' - \phi_1^2 \mathcal{U}) e^{i\phi + \sigma\mathcal{W}(t) - \frac{1}{2}\sigma^2 t}.\end{aligned} \tag{5}$$

Inserting equations (4) and (5) into equation (1), we get for imaginary part

$$(2\gamma_1\phi_1\xi_1 + \xi_3)\mathcal{U}' = 0. \tag{6}$$

Setting that:

$$\xi_3 = -2\gamma_1\phi_1\xi_1. \tag{7}$$

For real part

$$\begin{aligned}&(\gamma_1\xi_1^2)\mathcal{U}'' + (-\phi_3 - \gamma_1\phi_1^2)\mathcal{U} + \gamma_2\mathcal{U}\mathcal{V} e^{\sigma\mathcal{W}(t) - \frac{1}{2}\sigma^2 t} = 0,\\ &\gamma_3\xi_2\mathcal{V}' = \gamma_4\xi_1(\mathcal{U}^2)' e^{\sigma\mathcal{W}(t) - \frac{1}{2}\sigma^2 t}.\end{aligned} \tag{8}$$

Now, we take the expectation on both sides into equation (8) to get

$$(\gamma_1\xi_1^2)\mathcal{U}'' + (-\phi_3 - \gamma_1\phi_1^2)\mathcal{U} + \gamma_2\mathcal{U}\mathcal{V} e^{-\frac{1}{2}\sigma^2 t}\mathbb{E}(e^{\sigma\mathcal{W}(t)}) = 0, \tag{9}$$

and

$$\gamma_3\xi_2\mathcal{V}' = \gamma_4\xi_1(\mathcal{U}^2)' e^{-\frac{1}{2}\sigma^2 t}\mathbb{E}(e^{\sigma\mathcal{W}(t)}). \tag{10}$$

Using lemma 2, then equations (9- 10) turn into

$$(\gamma_1\xi_1^2)\mathcal{U}'' + (-\phi_3 - \gamma_1\phi_1^2)\mathcal{U} + \gamma_2\mathcal{U}\mathcal{V} = 0, \tag{11}$$

and

$$\gamma_3\xi_2\mathcal{V}' = \gamma_4\xi_1(\mathcal{U}^2)'. \tag{12}$$

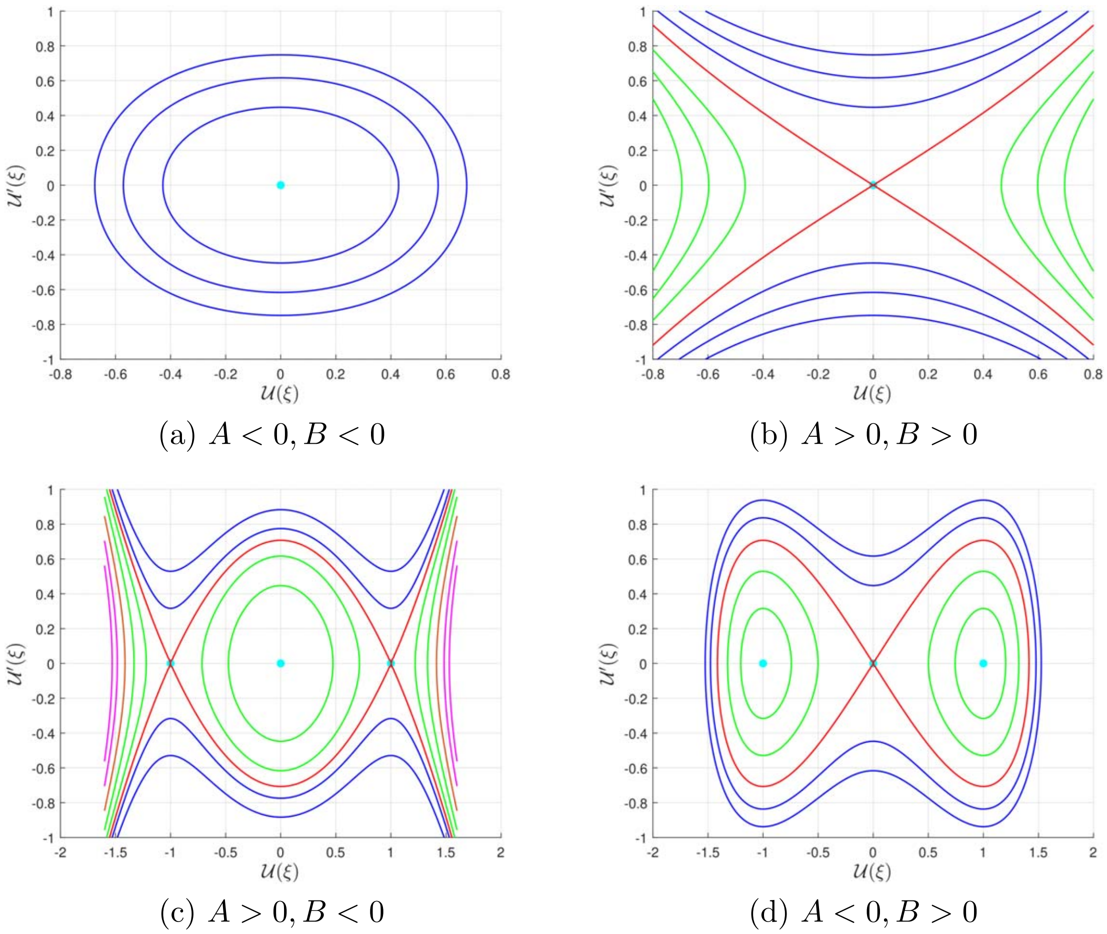

Figure 1. Phase portrait for the Hamiltonian system (15). The cyan solid point refers to the equilibrium point.

Integrating (12) once and ignoring the integral constant, we have

$$\mathcal{V} = \frac{\gamma_4 \xi_1}{\gamma_3 \xi_2} \mathcal{U}^2. \tag{13}$$

Substituting equation (13) into equation (11), we get

$$\mathcal{U}'' - A\mathcal{U}^3 - B\mathcal{U} = 0, \tag{14}$$

where

$$A = \frac{-\gamma_2 \gamma_4}{\gamma_3 \gamma_1 \xi_1 \xi_2} \text{ and } B = \frac{\phi_3 + \gamma_1 \phi_1^2}{\gamma_1 \xi_1^2}.$$

4. Hamiltonian system and phase portrait

Eq.(14) is rewritten as a system of first-order differential equations in the form

$$\mathcal{U}' = Z, \qquad Z' = A\mathcal{U}^3 + B\mathcal{U}. \tag{15}$$

This system is a Hamiltonian system because it can be driven by using Hamilton canonical equations with a Hamiltonian function in the form

$$H = \frac{1}{2} Z^2 - \frac{A}{4} \mathcal{U}^4 - \frac{B}{2} \mathcal{U}^2. \tag{16}$$

Due to $\frac{\partial H}{\partial \xi} = 0$, the Hamiltonian itself is a conserved quantity and it admits the form

$$\frac{1}{2} Z^2 - \frac{A}{4} \mathcal{U}^4 - \frac{B}{2} \mathcal{U}^2 = C, \tag{17}$$

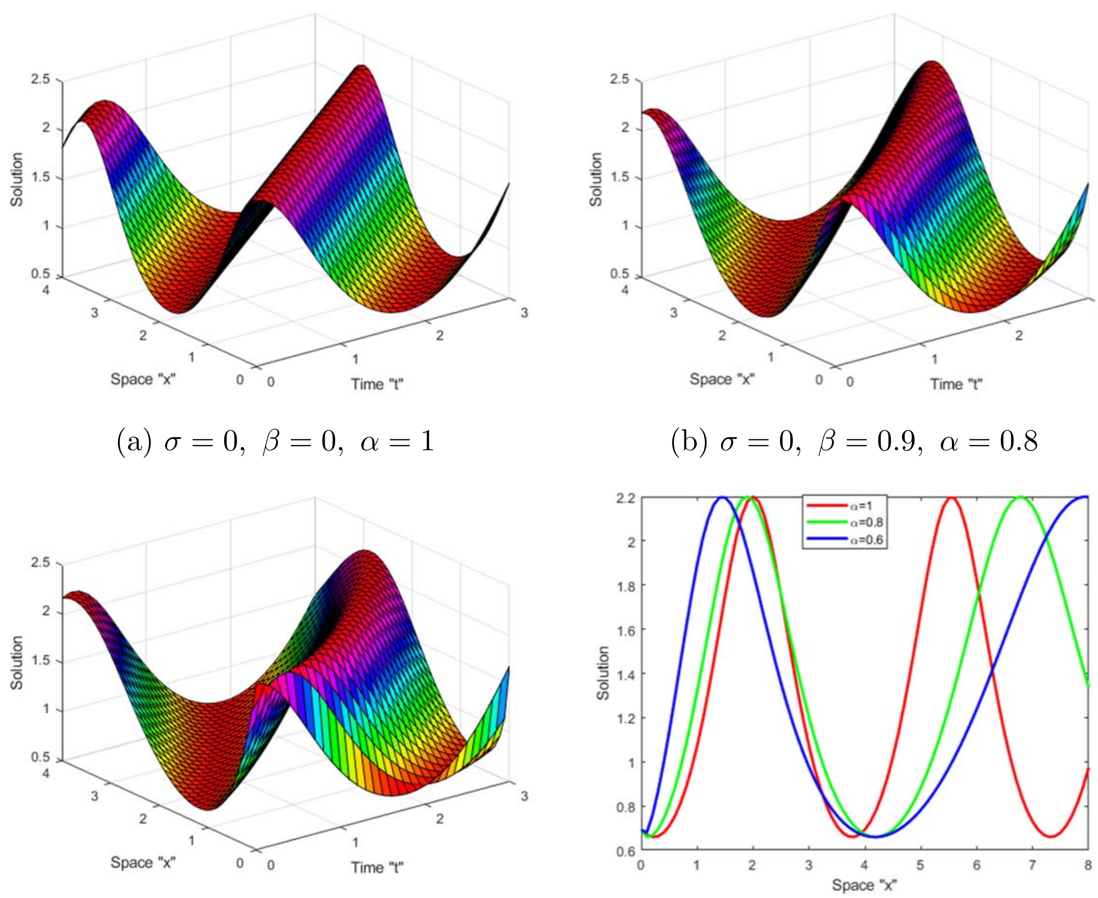

(a) $\sigma = 0,\ \beta = 0,\ \alpha = 1$ (b) $\sigma = 0,\ \beta = 0.9,\ \alpha = 0.8$

(c) $\sigma = 0,\ \beta = 0.9,\ \alpha = 0.6$ (d) $\sigma = 0,\ \alpha = 1,\ 0.8,\ 0.6$

Figure 2. (a)–(c) present the 3D-profile of the solution $\mathcal{Y}(x,\ y,\ t)$ to equation (33) with $\sigma = 0$ and various values of $\alpha = 1, 0.8, 0.6$ (d) illustrates a two-dimensional diagram for these α values.

where C is an arbitrary constant. Inserting the first equation in the system (15) into the conserved quantity and separating the variables, we get the one-dimension differential form

$$\frac{d\mathcal{U}}{\sqrt{Q(\mathcal{U})}} = \sqrt{2}\, d\xi, \tag{18}$$

where $Q(\mathcal{U})$ is quartic polynomial admitting the form

$$Q(\mathcal{U}) = C + \frac{A}{4}\mathcal{U}^4 + \frac{B}{2}\mathcal{U}^2. \tag{19}$$

The range of the parameters A, B, C is required for the integration of both sides of equation (18). We apply bifurcation analysis which was successfully applied in several works such as [43–46] to obtain this range. The bifurcation theory has many advantages such as it enables us to determine the type of the solutions before constructing them by employing the phase plane orbits and it helps us to form real and bounded solutions, that are desirable in real-world applications, by selecting possible intervals of real wave propagations. This method is easily applicable to Hamiltonian systems with small degrees of freedom. Its application becomes somewhat difficult as degrees of freedom increase, but the method is still applicable.

The equilibrium points (EQPs) for the Hamiltonian system (15) are acquired by setting $\mathcal{U}' = 0 = Z'$. They are $(\mathcal{U}_0,\ 0)$, where $\mathcal{U}_0$ satisfies the equation $A\mathcal{U}_0^3 + B\mathcal{U}_0 = 0$. Thus, system (15) has a single equilibrium point $O = (0, 0)$ if $BA > 0$, while it possess three EQPs $O = (0,\ 0)$, $P_{\pm} = (\pm\sqrt{\frac{-B}{A}},\ 0)$ if $BA < 0$. The determinant of the Jacobi matrix corresponding to the Hamiltonian system (15) has the form

$$\det\ [\mathrm{J}(\mathcal{U}_0,\ 0)] = 3A\mathcal{U}_0^2 + B. \tag{20}$$

According to the qualitative theory for planar integrable system [47], the equilibrium point $(\mathcal{U}_0,\ 0)$ is either saddle point if $\det\ [\mathrm{J}(\mathcal{U}_0,\ 0)] < 0$ or center point if $\det\ [\mathrm{J}(\mathcal{U}_0,\ 0)] > 0$, or cusp point if $\det\ [\mathrm{J}(\mathcal{U}_0,\ 0)] = 0$ besides the poincaré index of the equilibrium point is zero. Consequently, the unique equilibrium point O is center if $A < 0, B < 0$ and it is saddle if $B > 0, A > 0$. The EQPs O and $P_{\pm}$ are either center and saddle for $B < 0$,

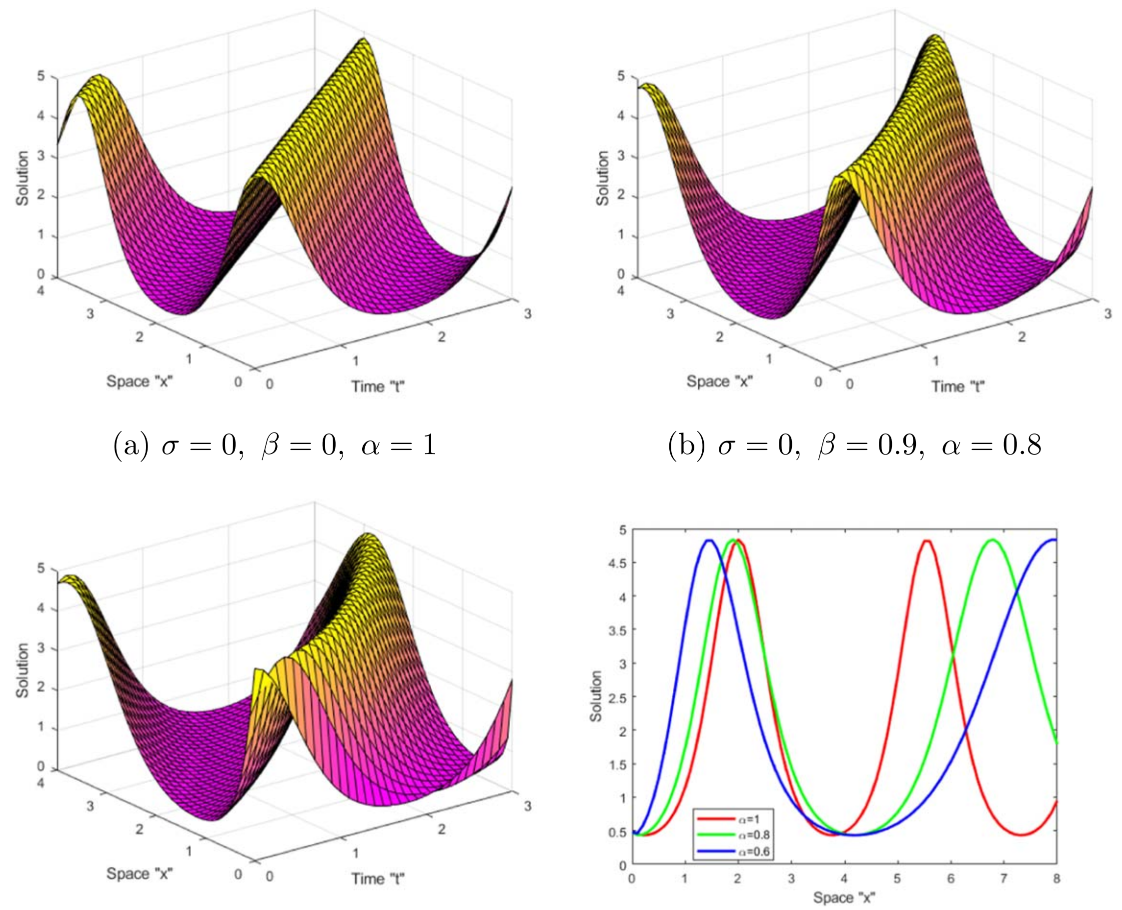

(a) $\sigma = 0,\ \beta = 0,\ \alpha = 1$ (b) $\sigma = 0,\ \beta = 0.9,\ \alpha = 0.8$

(c) $\sigma = 0,\ \beta = 0.9,\ \alpha = 0.6$ (d) $\sigma = 0,\ \alpha = 1,\ 0.8,\ 0.6$

Figure 3. (a)–(c) present the 3D-profile of $\mathcal{X}(x,\ y,\ t)$ presented in equation (34) with $\sigma = 0$ and various values of $\alpha = 1, 0.8, 0.6$ (d) illustrates a two-dimensional diagram for these α values.

$A > 0$ or saddle and center if $B > 0, A < 0$. To describe the phase portrait, we calculate the value of the constant C at the EQPs, i.e.,

$$C_0 = H(O) = 0, \qquad C_1 = H(P_{\pm}) = \frac{B^2}{4A}. \tag{21}$$

The phase plan orbits are one parameter family which is parameterized by the constant C and it admits the form

$$\mathcal{M}_C = \{(\mathcal{U},\ Z) \in \mathbb{R}^2\colon Z^2 = 2Q(\mathcal{U})\}. \tag{22}$$

We now give a short description of the phase portrait.

- For $(A,\ B) \in \mathbb{R}^- \times \mathbb{R}^-$, the system (15) possesses a family of bounded phase orbits, $\mathcal{M}_{C>0}$, around the centre point O. While $\mathcal{M}_{C=0}$, represents the equilibrium point O. This is outlined in figure 1(a).
- If $(A,\ B) \in \mathbb{R}^+ \times \mathbb{R}^+$, the phase portrait Includes three distinct unbounded families of phase orbits depending on the value of C. Two families of unbounded orbits in blue, $\mathcal{M}_{C>0}$ and in green $\mathcal{M}_{C<0}$. Both families are separated by the orbit $\mathcal{M}_{C=0}$ in red as clarified by figure 1(b).
- For $(A,\ B) \in \mathbb{R}^+ \times \mathbb{R}^-$, the phase portrait for the equation (15) is described by figure 1(c). If $C \in]0, C_1[$, there are three families of orbits in green. One of them is the bounded periodic family appearing inside the heteroclinic orbit $\mathcal{M}_{C=C_1}$ in red while the others are unbounded and they are placing outside the heteroclinic orbit. There is two unbounded families of orbits in blue $\mathcal{M}_{C>C_1}$, a single in brown $\mathcal{M}_{C=0}$, and two unbounded families $\mathcal{M}_{C<0}$ in pink exists.
- For $(A,\ B) \in \mathbb{R}^- \times \mathbb{R}^+$, the phase plane consists of bound orbits only as it is illustrated by figure 1(d). There is a family of supper periodic orbits in blue $\mathcal{M}_{C>0}$. There are two periodic families of orbits in green $\mathcal{M}_{C<0}$ and each of them is placed inside the right and left ovals of the homoclinic orbit $\mathcal{M}_{C=0}$ in red.

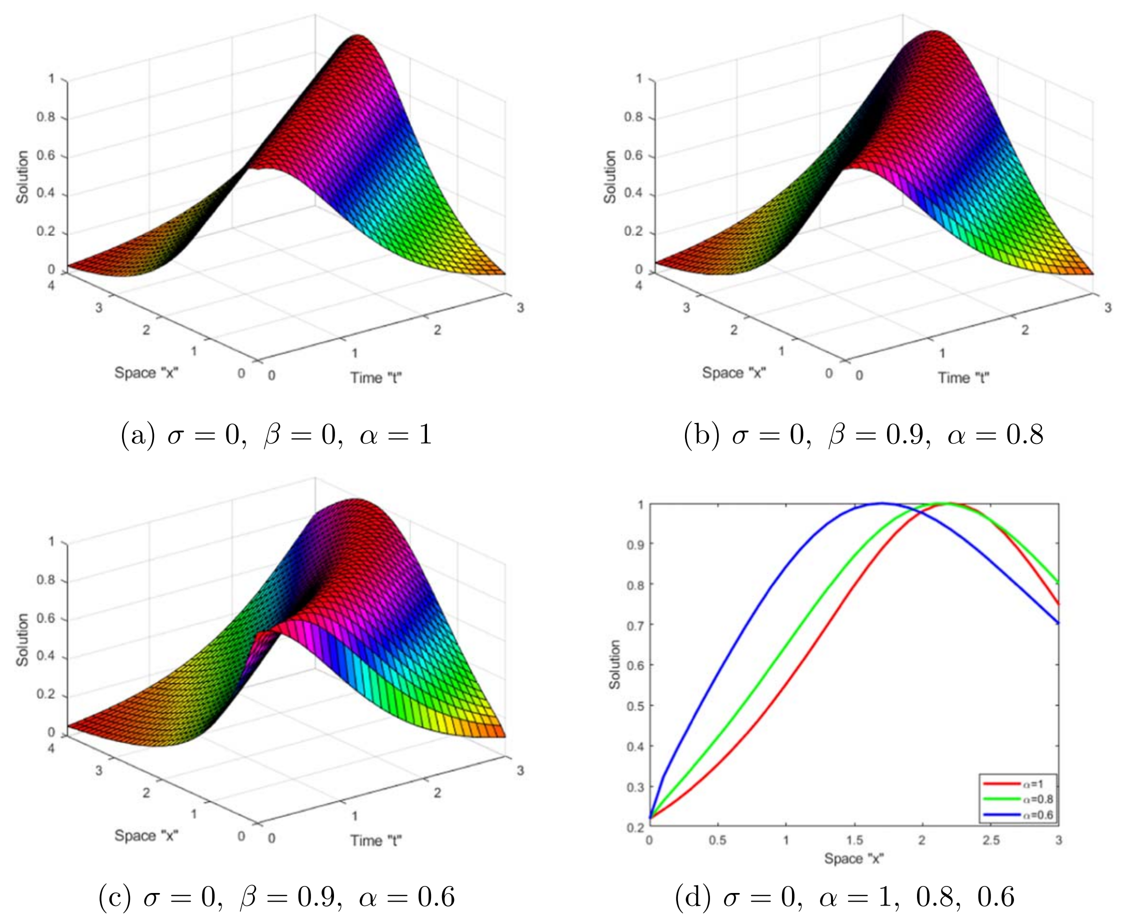

Figure 4. (a)–(c) display the 3D-profile of $\mathcal{Y}(x, y, t)$ presented in equation (36) with $\sigma = 0$ and distinct $\alpha = 1, 0.8, 0.6$ (d) illustrates a two-dimensional diagram for these α values.

5. Construction of the solutions

Depending on the bifurcation conditions of the parameters, and selecting the possible interval of real wave propagation, we introduce some solutions which are connected to bounded phase plan orbits.

1. For selecting values of A, B, and C that satisfy the condition $(A, B, C) \in \mathbb{R}^- \times \mathbb{R}^- \times]0, \infty[$, the system (15) has a family of periodic orbits each of them cuts $\mathcal{U}-$ axis in two points. This proves the quartic polynomial $Q(\mathcal{U})$ has only two real roots and hence, it takes the form $Q(\mathcal{U}) = -\frac{A}{4}(r_1^2 - \mathcal{U}^2)(r_2^2 + \mathcal{U}^2)$. The interval of real wave propagation is $\mathcal{U} \in]-r_1, r_1[$. Assuming $\mathcal{U}(0) = -r_1$, the integration of both sides of equation (18) provides

$$\mathcal{U}(\xi) = -r_1 \,\mathrm{cn}\left(\sqrt{\frac{-A}{2}(r_1^2 + r_2^2)}\,\xi, \frac{r_1}{r_1^2 + r_2^2}\right). \tag{23}$$

Consequently, the solution of SFFS (1) is

$$\mathcal{Y}(x, y, t) = -r_1 \,\mathrm{cn}\left(\sqrt{\frac{-A}{2}(r_1^2 + r_2^2)}\,\xi, \frac{r_1}{r_1^2 + r_2^2}\right) e^{i\phi + \sigma\mathcal{W}(t) - \frac{1}{2}\sigma^2 t}, \tag{24}$$

$$\mathcal{X}(x, y, t) = \frac{\gamma_4 \xi_1 r_1^2}{\gamma_3 \xi_2} \mathrm{cn}^2\left(\sqrt{\frac{-A}{2}(r_1^2 + r_2^2)}\,\xi, \frac{r_1}{r_1^2 + r_2^2}\right) e^{\sigma\mathcal{W}(t) - \frac{1}{2}\sigma^2 t}. \tag{25}$$

2. For $(A, B) \in \mathbb{R}^+ \times \mathbb{R}^-$, we have two possible choices according to the values of C as follows:

   (a) when $C < C_1$, there are three families of orbits in green. A single orbit of them intersects $\mathcal{U}$ in four points. This shows the polynomial Q has four real roots, namely, $\pm r_3, \pm r_4$. Then, it is written as $Q(\mathcal{U}) = \frac{A}{2}(r_3^2 - \mathcal{U}^2)(r_4^2 - \mathcal{U}^2)$, where $r_3 < r_4$. The interval of real wave propagation is

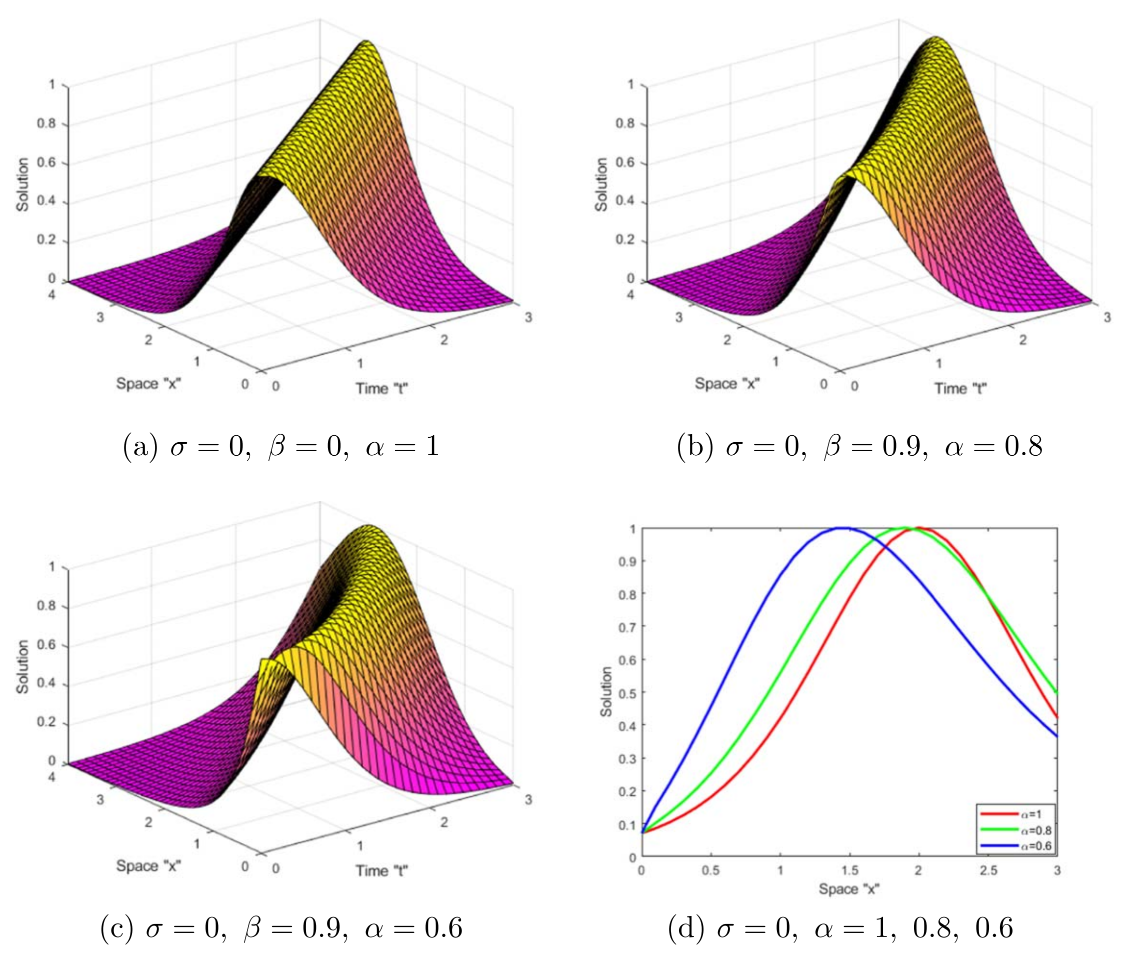

Figure 5. (a)–(c) display the 3D-profile of $\mathcal{X}(x,\ y,\ t)$ presented in equation (37) with $\sigma = 0$ and various values of $\alpha = 1, 0.8, 0.6$ (d) illustrates a two-dimensional diagram for these α values.

$\mathcal{U} \in]-r_3, r_3[\bigcup]r_4, \infty[\bigcup]-\infty, r_4[$. Assuming $\mathcal{U}(0) = -r_3$ and integrating both sides of equation (18), we obtain

$$\mathcal{U}(\xi) = \pm r_3 \mathrm{cd}\Big(r_4\sqrt{\frac{A}{2}}\xi,\ \frac{r_3}{r_4}\Big). \tag{26}$$

Therefore, the SFFS (1) has the solution

$$\mathcal{Y}(x,\ y,\ t) = \pm r_3 \mathrm{cd}\Big(r_4\sqrt{\frac{A}{2}}\xi,\ \frac{r_3}{r_4}\Big)e^{i\phi+\sigma\mathcal{W}(t)-\frac{1}{2}\sigma^2 t}, \tag{27}$$

$$\mathcal{X}(x,\ y,\ t) = \frac{\gamma_4\xi_1 r_3^2}{\gamma_3\xi_2}\mathrm{cd}^2\Big(r_4\sqrt{\frac{A}{2}}\xi,\ \frac{r_3}{r_4}\Big)e^{\sigma\mathcal{W}(t)-\frac{1}{2}\sigma^2 t}. \tag{28}$$

(b) When $C = C_1$, the system has a heteroclinic orbit which connects the two saddle points. The quartic polynomial (19) has the $\mathcal{U}-$ component of the equilibrium points as the roots. It is expressed as $Q\big(\mathcal{U}\big) = \frac{A}{4}\big(\frac{B}{A} + \mathcal{U}^2\big)^2$. The possible interval of bounded real wave propagation is $\mathcal{U} \in]-\sqrt{\frac{B}{A}},\ \sqrt{\frac{B}{A}}[$. Postulating $\mathcal{U}(0) = 0$, the integration of both sides of equation (18) provides

$$\mathcal{U}(\xi) = \sqrt{\frac{B}{A}}\tan\sqrt{\frac{B}{2}}\xi. \tag{29}$$

Consequently, the solution of the SFFS (1) is

$$\mathcal{Y}(x,\ y,\ t) = \sqrt{\frac{B}{A}}\tan\sqrt{\frac{B}{2}}\xi\, e^{i\phi+\sigma\mathcal{W}(t)-\frac{1}{2}\sigma^2 t}, \tag{30}$$

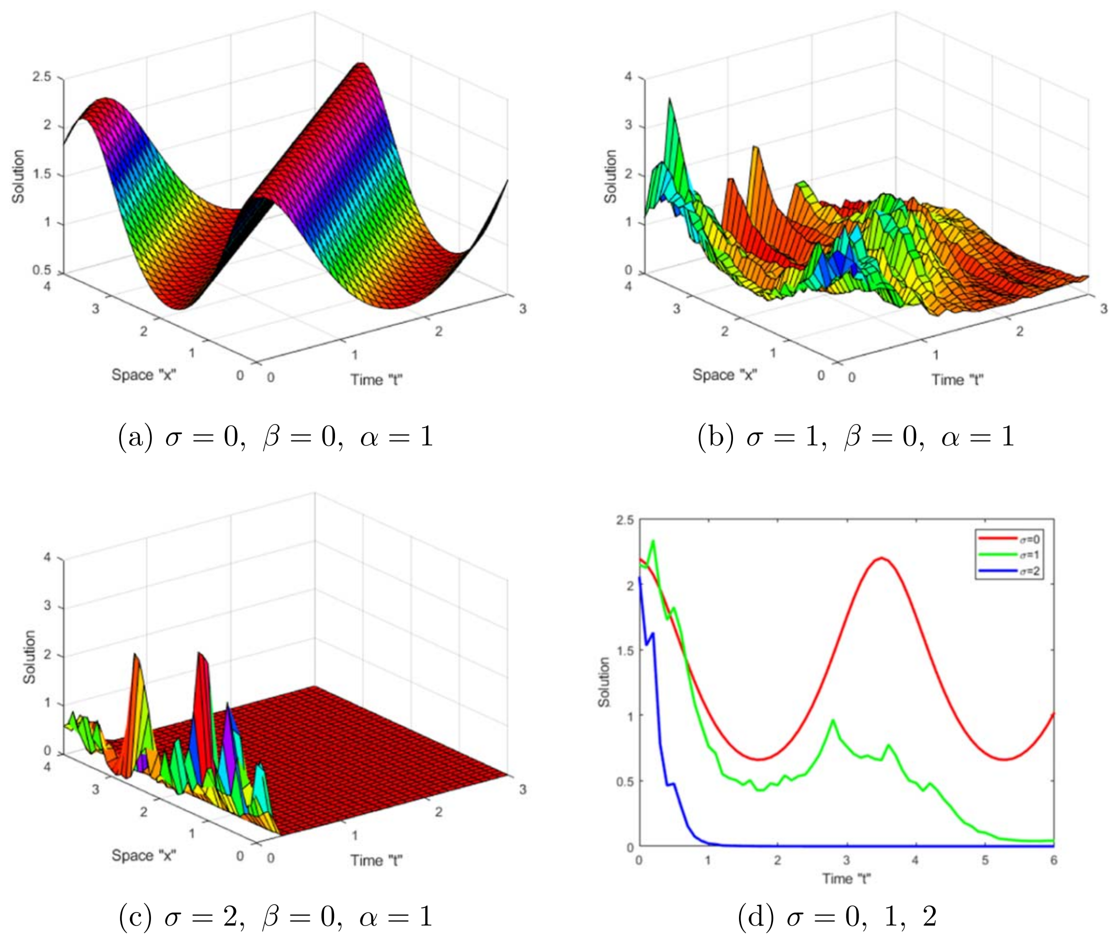

Figure 6. (a)–(c) display the 3D-profile of $\mathcal{Y}(x,\ y,\ t)$ presented in equation (33) for distinct values of $\sigma = 0, 1, 2$ (d) depicts a 2D graph for these σ values.

$$\mathcal{X}(x,\ y,\ t) = \frac{\gamma_4 \xi_1 B}{\gamma_3 \xi_2 A} \tan^2 \sqrt{\frac{B}{2}} \xi\, e^{\sigma \mathcal{W}(t) - \frac{1}{2}\sigma^2 t}. \tag{31}$$

3. For $(A,\ B) \in \mathbb{R}^- \times \mathbb{R}^+$, we have three possible cases according to the value of C:

   (a) The system (15) has a family of supper-periodic orbits when $C > 0$. Any orbit of this family $\mathcal{U}-$ axis in exactly two points. Therefore, the polynomial $Q(\mathcal{U})$ has two real roots, i.e., $Q(\mathcal{U}) = -\frac{A}{4}(r_5^2 - \mathcal{U}^2)(r_6^2 + \mathcal{U}^2)$. The interval of real wave propagation is $\mathcal{U} \in\ ]-r_5,\ r_5[$. Assuming $\mathcal{U}(0) = r_5$, the integration of both sides of Eq.(18) implies to

$$\mathcal{U}(\xi) = r_5\, \mathrm{cn}\left(\sqrt{\frac{-A}{2}(r_5^2 + r_6^2)}\,\xi,\ \frac{r_5}{\sqrt{r_5^2 + r_6^2}}\right). \tag{32}$$

   Hence, the solution of SFFS (1) has the form

$$\mathcal{Y} = r_5\, \mathrm{cn}\left(\sqrt{\frac{-A}{2}(r_5^2 + r_6^2)}\,\xi,\ \frac{r_5}{\sqrt{r_5^2 + r_6^2}}\right) e^{i\phi + \sigma \mathcal{W}(t) - \frac{1}{2}\sigma^2 t}, \tag{33}$$

$$\mathcal{X} = \frac{\gamma_4 \xi_1 r_5^2}{\gamma_3 \xi_2}\, \mathrm{cn}^2\left(\sqrt{\frac{-A}{2}(r_5^2 + r_6^2)}\,\xi,\ \frac{r_5}{\sqrt{r_5^2 + r_6^2}}\right) e^{\sigma \mathcal{W}(t) - \frac{1}{2}\sigma^2 t}. \tag{34}$$

   (b) For $C = 0$, the system (15) has homoclinic orbit which cuts $\mathcal{U}-$ axis in three point. Hence the polynomial Q possesses three real roots; one is repeated twice while the others are simple. So, we write $Q(\mathcal{U}) = -\frac{A}{4}\mathcal{U}^2(-\frac{2B}{A} - \mathcal{U}^2)$. The intervals of permitted wave propagation are

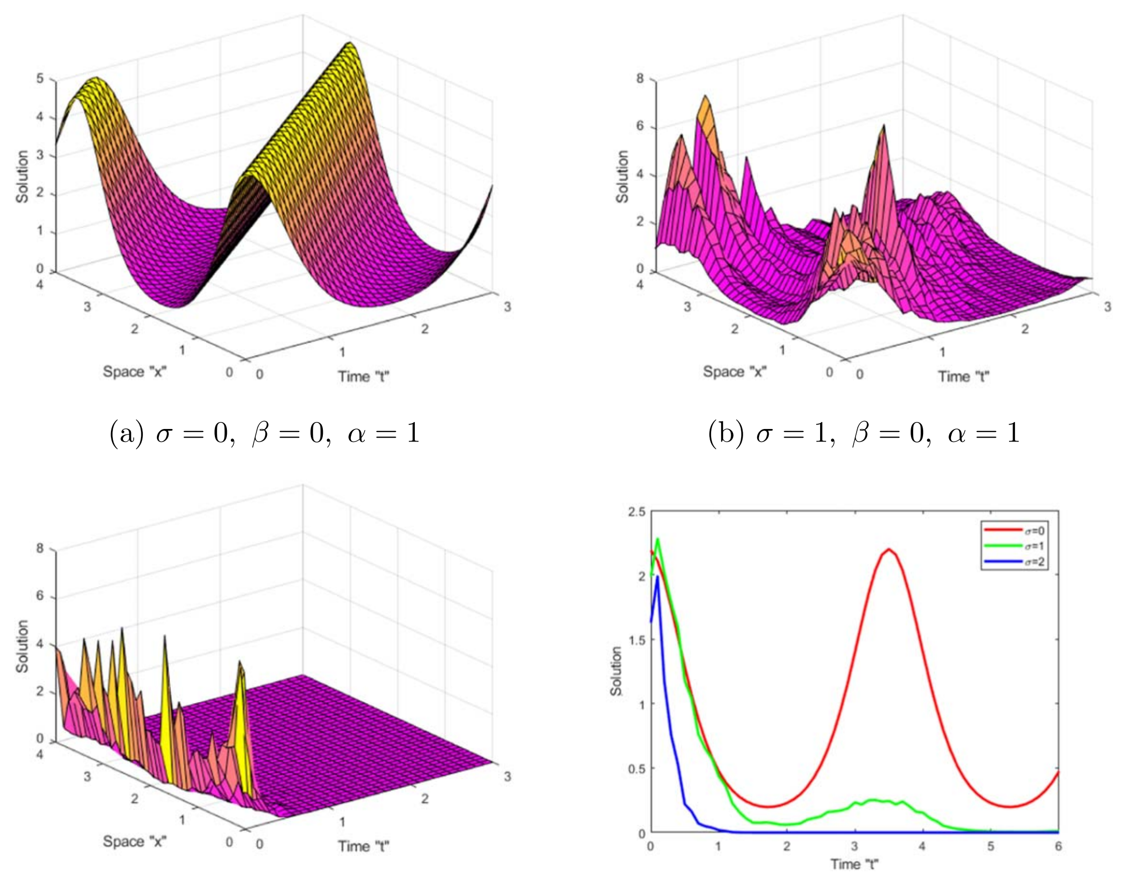

(a) $\sigma = 0,\ \beta = 0,\ \alpha = 1$ (b) $\sigma = 1,\ \beta = 0,\ \alpha = 1$

(c) $\sigma = 2,\ \beta = 0,\ \alpha = 1$ (d) $\sigma = 0,\ 1,\ 2$

Figure 7. (a)–(c) display the 3D-profile of $\mathcal{X}(x,\ y,\ t)$ presented in equation (34) for distinct values of $\sigma = 0, 1, 2$ (d) shows a 2D graph for these σ values.

$\mathcal{U} \in \left]-\sqrt{\frac{-2B}{A}}, 0\right[\bigcup\left]0, \sqrt{\frac{-2B}{A}}\right[$. Let $\mathcal{U}(0) = \sqrt{\frac{-2B}{A}}$ and integrating both sides of equation (18), we have

$$\mathcal{U}(\xi) = \sqrt{\frac{-2B}{A}}\ \mathrm{sech}\left(\sqrt{\frac{-A}{2}}\,\xi\right). \tag{35}$$

Consequently, the solution of the SFFS (1) is

$$\mathcal{Y}(x,\ y,\ t) = \sqrt{\frac{-2B}{A}}\ \mathrm{sech}\left(\sqrt{\frac{-A}{2}}\,\xi\right)e^{i\phi+\sigma\mathcal{W}(t)-\frac{1}{2}\sigma^2 t}, \tag{36}$$

$$\mathcal{X}(x,\ y,\ t) = \frac{-2\gamma_4\xi_1 B}{\gamma_3\xi_2 A}\ \mathrm{sech}^2\left(\sqrt{\frac{-A}{2}}\,\xi\right)e^{\sigma\mathcal{W}(t)-\frac{1}{2}\sigma^2 t}. \tag{37}$$

(c) The system (15) owns two families of periodic orbits in which any orbit of this family cuts $\mathcal{U}-$ axis in four points. This means the quartic polynomial (19) has four real roots. Consequently, $Q(\mathcal{U}) = -\frac{A}{4}(r_7^2 - \mathcal{U}^2)(\mathcal{U}^2 - r_8^2)$, where $0 < r_7 < r_8$. The intervals of real wave propagation are $\mathcal{U} \in \left]r_7, r_8\right[\bigcup\left]-r_8, -r_7\right[$. Assuming $\mathcal{U}(0) = r_7$, the integration of both sides of equation (18) produces

$$\mathcal{U}(\xi) = r_7\,\mathrm{nd}\left(\sqrt{\frac{-A}{2}}\,\xi,\ \sqrt{1 - \frac{r_7^2}{r_8^2}}\right). \tag{38}$$

So, the solution of the SFFS (1) is

$$\mathcal{Y}(x,\ y,\ t) = r_7\,\mathrm{nd}\left(\sqrt{\frac{-A}{2}}\,\xi,\ \sqrt{1 - \frac{r_7^2}{r_8^2}}\right)e^{i\phi+\sigma\mathcal{W}(t)-\frac{1}{2}\sigma^2 t}, \tag{39}$$

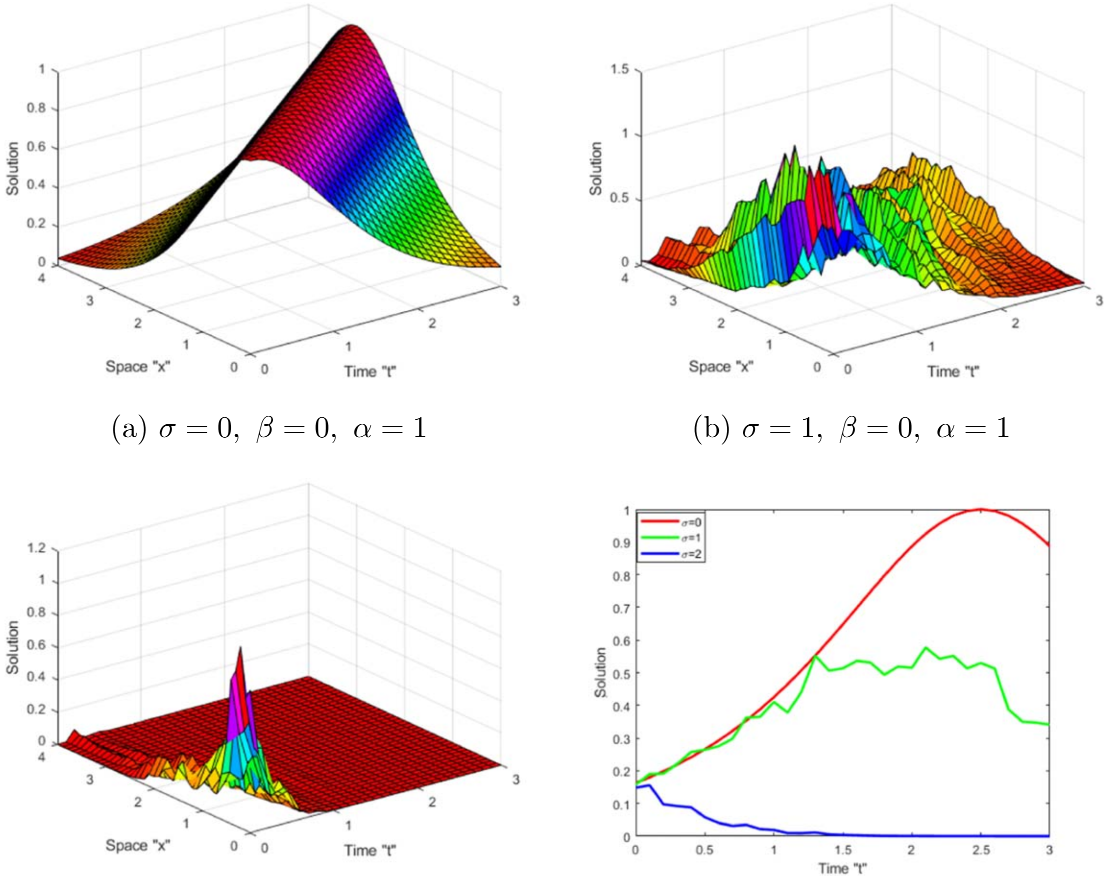

(a) $\sigma = 0,\ \beta = 0,\ \alpha = 1$ (b) $\sigma = 1,\ \beta = 0,\ \alpha = 1$

(c) $\sigma = 2,\ \beta = 0,\ \alpha = 1$ (d) $\sigma = 0,\ 1,\ 2$

Figure 8. (a)–(c) display the 3D-profile of $\mathcal{Y}(x,\ y,\ t)$ presented in equation (36) for distinct values of $\sigma = 0, 1, 2$ (d) shows a 2D graph for these σ values.

$$\mathcal{X}(x,\ y,\ t) = \frac{\gamma_4 \xi_1 r_7^2}{\gamma_3 \xi_2} \mathrm{nd}^2\left(\sqrt{\frac{-A}{2}}\,\xi,\ \sqrt{1 - \frac{r_7^2}{r_8^2}}\right) e^{\sigma \mathcal{W}(t) - \frac{1}{2}\sigma^2 t}. \tag{40}$$

6. Impacts of noise and MTD

We examine the influence of the MTD and the stochastic term on the analytical solutions of the SFFS (1). To show the behavior of these solutions, numerous graphical representations are provided. For varying values of σ (amplitude of noise) and α (the order of derivatives), we simulate a number of figures for attained solutions, for example, equations (33), (34), (36) and (37).

Impacts of MTD: In figures 2, 3, 4 and 5 if $\sigma = 0$, we notice that the shape of the graph is shrinking as the value of α increases:

As we can see in figures 2, 3, 4, and 5, the solution curves do not intersect. Additionally, the curves shrink when the order of the derivative increases.

Impact of the noise: The impact of noise on the solutions is seen in figures 6, 7, 8 and 9 as follows:

From figures 5, 6, 7, and 8, we may infer that when the noise is ignored (i.e. at $\sigma = 0$), there are various solutions, such as periodic solutions, kinked solutions, and others. As shown by the 2D graph, the addition of noise with an amplitude of $\sigma = 1, 2$ causes the surface to become significantly flattened after tiny transit patterns. This indicates that when the stochastic term is included, the solutions of SFFS (1) converge to zero.

7. Conclusions

In this paper, the stochastic fractional Fokas system (SFFS) with M-truncated derivatives. Utilizing the conserved quantity, we constructed some new traveling wave solutions for the SFFS (1). These solutions can

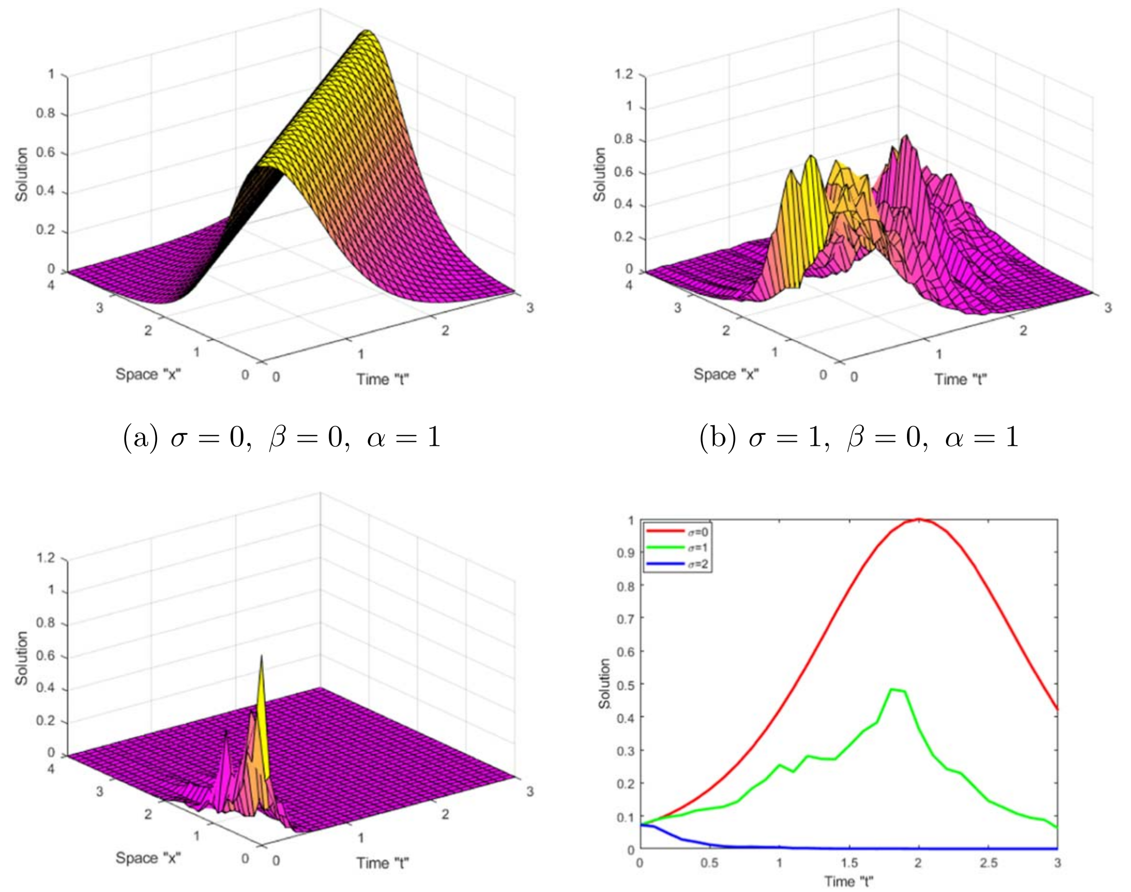

(a) $\sigma = 0,\ \beta = 0,\ \alpha = 1$ (b) $\sigma = 1,\ \beta = 0,\ \alpha = 1$

(c) $\sigma = 2,\ \beta = 0,\ \alpha = 1$ (d) $\sigma = 0,\ 1,\ 2$

Figure 9. (a)–(c) present the 3D-profile of $\mathcal{X}(x,\ y,\ t)$ presented in equation (37) for distinct values of $\sigma = 0, 1, 2$ (d) shows a 2D graph for these σ values.

clarify a variety of fascinating and intricate physical phenomena due to the use of the Fokas system in describing nonlinear pulse propagation in mono-mode optical fibers. Additionally, the multiplicative noise has an impact on the analytical solution of SFFS (1). We deduced that the multiplicative noise stabilizes solutions at zero. On the other side, we noticed that the M-truncated derivatives shrink the surface as the order of derivative α increases.

The bifurcation method which has been employed to find the solutions is successfully and easily applicable to find the solution of PDEs and its extension to SFPDEs when the reduced ordinary differential equation is expressed as one-dimensional Hamiltonian system. The difficulty if its application arises when the dimension of such Hamiltonian system increases because it requires investigation the integrability of the Hamiltonian system and constructing the additional integrals of motion which is not an easy task.

Acknowledgments

This research has been funded by the Scientific Research Deanship at the University of Ha'il-Saudi Arabia through project number RG-23026.

Data availability statement

All data that support the findings of this study are included within the article (and any supplementary files).

Disclosure statement

No potential conflict of interest was reported by the authors.

ORCID iDs

Wael W Mohammed https://orcid.org/0000-0002-1402-7584
Adel A Elmandouh https://orcid.org/0000-0002-7191-2010

References

[1] Arnold L 1998 *Random Dynamical Systems* (Springer)
[2] Imkeller P and Monahan A H 2002 Conceptual stochastic climate models *Stoch. Dyn.* **2** 311–26
[3] Mohammed W W, Al-Askar F M and Cesarano C 2022 On the dynamical behavior of solitary waves for coupled stochastic korteweg-de vries equations *ZAMM J. Appl. Math. Mech.* **103** e202100199
[4] Mohammed W W, Al-Askar F M and Cesarano C 2022 The analytical solutions of the stochastic mKdV equation via the mapping method *Mathematics* **10** 4212
[5] Al-Askar F M, Cesarano C and Mohammed W W 2022 Multiplicative brownian motion stabilizes the exact stochastic solutions of the davey-stewartson equations *Symmetry* **14** 2176
[6] Mohammed W W and Cesarano C 2023 The soliton solutions for the $(4+1)$-dimensional stochastic Fokas equation *Math. Methods Appl. Sci.* **46** 7589–97
[7] Oldham K B and Spanier J 1974 *The fractional calculus: Theory and applications of differentiation and integration to Arbitrary Order, vol. 11 of Mathematics in Science and Engineering* (Academic)
[8] Miller K and Ross B 1993 *An Introduction to the Fractional Calculus and Fractional Differential Equations* (Wiley)
[9] Podlubny I 1999 *Fractional Differential Equations, vol. 198 of Mathematics in Science and Engineering* (San Diego, Calif, USA: Academic)
[10] Hilfer R 2000 *Applications of Fractional Calculus in Physics* (World Scientific Publishing)
[11] Oustaloup A 1991 *La Commande CRONE: Commande Robuste d'Ordre Non Entier* (Editions Hermès)
[12] Mouy M, Boulares H, Alshammari S, Alshammari M and Laskri Y 2023 On averaging principle for caputo-hadamard fractional stochastic differential pantograph equation *Fractal and Fractional* **7** 31
[13] Kilbas A A, Srivastava H M and Trujillo J J 2016 *Theory and Applications of Fractional Differential Equations* (Elsevier) 2016
[14] Samko S G, Kilbas A A and Marichev O I 1993 *Fractional Integrals and Derivatives, Theory and Applications* (Gordon and Breach)
[15] Elias-Zuniga A 2022 On the two-scale dimension and its application for deriving a new analytical solution for the fractal Duffing's equation *Fractals* **30** 2250061
[16] He J H 2011 A new fractal derivation *Therm. Sci.* **15** 145–7
[17] Atangana A and Baleanu D 2016 New fractional derivatives with nonlocal and non-singular kernal: theory and applications to heat transfer model *Therm. Sci.* **20** 761–9
[18] Sousa J V and De Oliveira E C 2018 A new truncated M-fractional derivative type unifying some fractional derivative types with classical properties *International Journal of Analysis and Applications* **16** 83–96
[19] Jawad A J M, Petković M D and Biswas A 2010 Modified simple equation method for nonlinear evolution equations *Appl. Math. Comput.* **217** 869–77
[20] Lu B 2012 The first integral method for some time fractional differential equations *J. Math. Anal. Appl.* **395** 684–93
[21] Zheng B 2012 G'/G)-expansion method for solving fractional partial differential equations in the theory of mathematical physics *Commun. Theor. Phys.* **58** 623–30
[22] Sonmezoglu A 2015 Exact solutions for some fractional differential equations *Advances in Mathematical Physics* **2015** 567842
[23] Al-Askar F M and Mohammed W W 2023 Abundant optical solutions for the Sasa-Satsuma equation with M-truncated derivative *Frontiers in Physics* **11** 1216451
[24] Eslami M, Vajargah B F, Mirzazadeh M and Biswas A 2014 Application of first integral method to fractional partial differential equations *Indian J. Phys.* **88** 177–84
[25] Eslami M and Rezazadeh H 2016 The first integral method for Wu-Zhang system with conformable time-fractional derivative *Calcolo.* **53** 475–85
[26] Mirzazadeh M, Eslami M, Zerrad E, Mahmood M F, Biswas A and Belic M 2015 Optical solitons in nonlinear directional couplers by sine-cosine function method and Bernoulli's equation approach *Nonlinear Dyn.* **81** 1933–49
[27] Ur Rehman H, Iqbal I, Hashemi M S, Mirzazadeh M and Eslami M 2023 Analysis of cubic-quartic-nonlinear Schrödinger's equation with cubic-quintic-septic-nonic form of self-phase modulation through different techniques *Optik* 171028
[28] Liu J G, Zhu W H, Wu Y K and Jin G H 2023 Application of multivariate bilinear neural network method to fractional partial differential equations *Results in Physics* **47** 106341
[29] Fokas A S 1994 On the simplest integrable equation in $2+1$ *Inverse Prob.* **10** L19
[30] Shulman E I 1983 On the integrability of equations of Davey Stewartson type *Teor. Mat. Fiz.* **56** 131–6
[31] Kaplan M, Akbulut A and Alqahtani R T 2023 New solitary wave patterns of the fokas system in fiber optics *Mathematics* **11** 1810
[32] Zhang P L and Wang K J 2022 Abundant optical soliton structures to the Fokas system arising in monomode optical fibers *Open Physics* **20** 493–506
[33] Wang K J 2022 Abundant exact soliton solutions to the Fokas system *Optik* **2022** 168265
[34] Tarla S, Ali K K, Sun T C, Yilmazer R and Osman M S 2022 Nonlinear pulse propagation for novel optical solitons modeled by Fokas system in monomode optical fibers *Results Phys.* **36** 1053
[35] Mohammed W W, Cesarano C, Elsayed E M and Al-Askar F M 2023 The analytical fractional solutions for coupled Fokas system in fiber optics using different methods *Fractal and Fractional.* **7** 556
[36] Wang K J, Liu J H and Wu J 2022 Soliton solutions to the Fokas system arising in monomode optical fibers *Optik* **251** 168319
[37] Mohammed W W, Al-Askar F M and Cesarano C 2023 Solitary Solutions for the Stochastic Fokas System Found in Monomode Optical Fibers *Symmetry* **15** 1433
[38] Rao J, Mihalache D, Cheng Y and He J 2019 Lump-soliton solutions to the Fokas system *Phys Lett A* **383** 1138–42
[39] Verma P and L Kaur L 2021 New exact solutions of the (4+1)-dimensional Fokas equation via extended version of $exp(-\psi(k))$ -expansion method *Int. J. Comput. Appl.* **7** 104
[40] Tan W, Dai Z D and Qiu D Q 2018 Parameter limit method and its application in the (4+1)-dimensional Fokas equation *Computers and Mathematics with Applications* **75** 4214–20

[41] Murad M A S, Hamasalh F K and Ismael H I 2023 Optical soliton solutions for time-fractional Fokas system in optical fiber by new Kudryashov approach *Optik* **280** 170784
[42] Calin O 2015 *An Informal Introduction to Stochastic Calculus with Applications* (World Scientific Publishing Co. Pte. Ltd)
[43] El-Dessoky M M and Elmandouh A A 2023 Qualitative analysis and wave propagation for Konopelchenko-Dubrovsky equation *Alex. Eng. J.* **67** 525–35
[44] Elbrolosy M E and Elmandouh A A 2022 Construction of new traveling wave solutions for the (2. 1) dimensional extended Kadomtsev-Petviashvili equation *J. Appl. Anal. Comput.* **12** 533–50
[45] Elmandouh A A and Fadhal E 2022 Bifurcation of Exact Solutions for the Space-Fractional Stochastic Modified Benjamin-Bona-Mahony Equation *Fractal and Fractional* **12** 718
[46] Elbrolosy M E 2021 Qualitative analysis and new soliton solutions for the coupled nonlinear Schrödinger type equations *Phys. Scr.* **96** 125275
[47] Nemytskii V V and Stepanov V V 1960 Qualitative theory of differential equations *Princeton Mathematical Series, No. 22* (Princeton University Press) p 523